Vortex charge in mesoscopic superconductors

S. V. Yampolskii,* B. J. Baelus, and F. M. Peeters†
Departement Natuurkunde, Universiteit Antwerpen (UIA), Universiteitsplein 1, B-2610 Antwerpen, Belgium

J. Koláček
Institute of Physics, ASCR, Cukrovarnická 10, Prague 6, Czech Republic

(Received 14 November 2000; revised manuscript received 4 May 2001; published 21 September 2001)

The electric charge density in mesoscopic superconductors with circular symmetry, i.e., disks and cylinders, is studied within the phenomenological Ginzburg-Landau approach. We found that even in the Meissner state there is a charge redistribution in the sample which makes the sample edge become negatively charged. In the vortex state there is a competition between this Meissner charge and the vortex charge which may change the polarity of the charge at the sample edge with increasing magnetic field. It is shown analytically that in spite of the charge redistribution the mesoscopic sample as a whole remains electrically neutral.

DOI: 10.1103/PhysRevB.64.144511 PACS number(s): 74.20.De, 74.60.Ec, 41.20.Cv

I. INTRODUCTION

The idea of ''an electric charge associated with a vortex'' was proposed many years ago. In fact, it arised from London's prediction that in superconductors with a nonuniform distribution of the superconducting current an electric field is associated.[1] This phenomenon is similar to the hydrostatic Bernoulli effect[2] and leads to the appearance of an electrostatic potential difference inside the sample. This Bernoulli potential compensates at each point of the superconductor the kinetic shift of the chemical potential of the electrons, which is associated with the kinetic energy of the superconducting condensate, so that the electrochemical potential of the electrons remains constant in space. Ivanchenko and Omel'yanchuk[3] predicted, for bulk superconductors in an external magnetic field, that an electrical polarization is induced by this Bernoulli effect. They also calculated the polarization moment of a superconductor, the quadrupole moment for a sphere, and the dipole moment for a distorted sphere. When the vortex exists in the bulk of a superconductor the Bernoulli potential creates an additional force which balances the inertial and Lorentz forces acting on the vortex.[4]

Interest in this subject reappeared when Khomskii and Freimuth[5] showed that the vortex in a high-temperature superconductor (HTS) can accumulate a finite electric charge. This effect occurs because of the difference of the chemical potential in the superconducting condensate versus the normal state (vortex core). Such a change in chemical potential (which is similar to the above Bernoulli effect) results in a redistribution of the electrons in the region near the vortex and culminates in a charging of the vortex core. Later the same effect was predicted for a single Abrikosov vortex in a type-II bulk superconductor[6,7] and very recently for the flux line lattice in a bulk superconductor.[8] Recently, the vortex charge was also studied for other superconducting systems, such as the Bose liquid,[9] unconventional superconducting materials: with hole superconductivity[10] and chiral *p*-wave superconductors.[11] At last, at the end of 2000 the first experimental evidence of vortex core charge was obtained in HTS's by high-resolution measurements of the nuclear quadrupole frequency which is very sensitive to the local charge density.[12]

In the present paper we investigate this phenomenon in mesoscopic superconductors. All previous papers on this subject dealt with bulk superconductors. A mesoscopic sample has a typical size which is comparable to the coherence length (ξ) and the magnetic field penetration depth (λ). The behavior of such structures in an external magnetic field (H) is strongly influenced by the sample shape[13,14] and may lead to various superconducting states and different phase transitions between them. Jumps in magnetization were observed when the applied magnetic field or temperature (T) is varied.[15]

A number of earlier works studied the geometry-dependent magnetic response of mesoscopic superconductors: (i) disk-shaped samples,[16–22] (ii) infinitely long cylinders,[23,24] and (iii) ringlike structures[25,26] and more complicated geometries.[27] Theoretical studies of mesoscopic superconductors are based on the phenomenological Ginzburg-Landau (GL) theory[28] which successfully describes mesoscopic samples in a wide H-T region. In particular, it has been shown that in mesoscopic samples (disks or cylinders) surrounded by a vacuum or an insulator two kinds of superconducting states can exist. First, there is a circular symmetric state with a fixed value of angular momentum, called giant vortex. The observed magnetization jumps correspond to first-order phase transitions between giant vortices with different angular momentum.[16,17] Second, in samples with a sufficiently large radius multivortex structures[18] can nucleate which are the analog of the Abrikosov flux line lattice in a bulk superconductor. These states can be represented as a mixture of giant vortex states with different angular momentum. For multivortex states it is also possible to introduce an effective total angular momentum, which is nothing else than the number of vortices in the disk, i.e., the vorticity. With changing the magnetic field there is a second-order phase transition between the multivortex and the giant vortex state.[18,19,29]

It is expected that the charge distribution in such mesoscopic samples may be appreciably altered due to the presence of a boundary. Furthermore, screening currents near the

boundary of the sample will also lead to a redistribution of charge and consequently even in the Meissner state there will be a nonuniform distribution in the sample. In a certain sense, this case can be viewed as a vortex turned inside out, i.e., with its core at infinity. In the presence of vortices there will be an interplay between the Meissner charge and the previously studied[5,6,8] vortex charge which is unique for mesoscopic samples.

The present paper is organized as follows. In Sec. II we give the necessary theoretical formalism on which our numerical results are based. In Sec. III we investigate the charge distribution in both the Meissner state and the giant vortex states. Then the charge distribution in the multivortex state is discussed for thin disks (Sec. IV). In Sec. V we summarize our results and briefly discuss a possibility of their experimental detection. In the Appendix we present the proof of electrical neutrality in a mesoscopic superconductor of general shape.

II. THEORETICAL APPROACH

We consider a mesoscopic superconducting sample of circular symmetry with radius R and thickness d surrounded by an insulating medium. The external magnetic field $\vec{H}=(0,0,H)$ is uniform and directed normal to the superconductor plane. The starting point of our analysis is that the rotating motion of Cooper pairs around the vortex core leads to a spatial redistribution of charge carriers, which generate the electrostatic potential[5,6,8]

$$\varphi(\vec{r})=\varphi_0[|\psi(\vec{r})|^2-1], \tag{1}$$

where $\psi(\vec{r})$ is the dimensionless superconducting order parameter normalized so that $|\psi(\vec{r})|^2$ is measured in units of the Cooper pair density in a bulk superconductor. The amplitude φ_0 is different in different approaches. We use $\varphi_0=|\alpha|/2e$ as proposed in Ref. 8. A 3-times smaller value $\varphi_0=|\alpha|/6e$ was used in Ref. 5. From the theory in Ref. 6 it follows approximately that $\varphi_0=(|\alpha|/2\pi^2 e)(dT_c/d\ln\epsilon_F)$, where $dT_c/d\ln\epsilon_F\approx\ln(\hbar\omega_D/k_BT_c)\sim 1$–10. Thus all approaches yield an electrostatic potential of a similar magnitude.

The distribution of the corresponding charge density $q(\vec{r})$ is obtained from the Poisson equation[30]

$$4\pi q(\vec{r})=-\vec{\nabla}^2\varphi(\vec{r}). \tag{2}$$

The Cooper pair density $|\psi(\vec{r})|^2$ is determined from a solution of the system of two coupled nonlinear GL equations for the superconducting order parameter, $\psi(\vec{r})$, and the magnetic field [or vector potential $\vec{A}(\vec{r})$]

$$(-i\vec{\nabla}-\vec{A})^2\psi=\psi-\psi|\psi|^2, \tag{3}$$

$$\kappa^2\vec{\nabla}\times\vec{\nabla}\times\vec{A}=\vec{j}, \tag{4}$$

where the density of the superconducting current $\vec{j}$ is given by

$$\vec{j}=\frac{1}{2i}(\psi^*\vec{\nabla}\psi-\psi\vec{\nabla}\psi^*)-|\psi|^2\vec{A}. \tag{5}$$

Here $\vec{r}=(\vec{\rho},z)$ is the three-dimensional position in space. Due to the circular symmetry of the sample, we use cylindrical coordinates: ρ is the radial distance from the disk center, θ is the azimuthal angle, and the z axis is taken perpendicular to the disk plane, where the disk lies between $z=-d/2$ and $z=d/2$. For $d\to\infty$ we obtain the cylinder geometry. All distances are measured in units of the coherence length $\xi=\hbar/\sqrt{2m^*|\alpha|}$ ($m^*=2m$ is the mass of the Cooper pair), the vector potential in $c\hbar/2e\xi$, the magnetic field in $H_{c2}=c\hbar/2e\xi^2=\kappa\sqrt{2}H_c$, where H_c is the thermodynamical critical field, and the superconducting current in $j_0=cH_c/2\pi\xi$, and $\kappa=\lambda/\xi$ is the GL parameter.

Equations (3)–(5) have to be supplemented by boundary conditions for $\psi(\vec{r})$ and $\vec{A}(\vec{r})$. For the superconducting condensate it can be written as[28]

$$\vec{n}\cdot(-i\vec{\nabla}-\vec{A})\psi|_S=0, \tag{6}$$

where $\vec{n}$ is the unit vector normal to the sample surface. The boundary condition for the vector potential has to be taken far away from the superconductor where the magnetic field becomes equal to the external applied field H:

$$\vec{A}|_{r\to\infty}=\frac{1}{2}H\rho\vec{e}_\theta, \tag{7}$$

where $\vec{e}_\theta$ denotes the azimuthal direction.

The free energy of the superconducting state, measured in $F_0=H_c^2V/8\pi$ units, is determined by the expression

$$F=\frac{2}{V}\left\{\int dV\left[-|\psi|^2+\frac{1}{2}|\psi|^4+|-i\vec{\nabla}\psi-\vec{A}\psi|^2+\kappa^2[\vec{h}(\vec{r})-\vec{H}]^2\right]\right\}, \tag{8}$$

with the magnetic field

$$\vec{h}(\vec{r})=\vec{\nabla}\times\vec{A}(\vec{r}).$$

Here we will consider three different geometries for the superconductor: (I) an infinitely long cylinder, (II) a thin disk with finite thickness $d\lesssim\lambda,\xi$, and (III) an infinitely thin disk, i.e., $d\to 0$. In all three cases the superconducting order parameter does not depend on z. In case I it obviously follows from the sample geometry. In cases II and III it was found[17] that the dependence of $\psi(\vec{r})$ on z is very slow. This allows us to average $\psi(\vec{r})$ over the sample thickness and to solve the problem for the two-dimensional problem for the order parameter $\psi(\rho,\theta)$. However, the magnetic field in case II has a z dependence, which is responsible for the demagnetization effect. For both cases I and II we solve the problem numerically by the method proposed in Ref. 17. For thin mesoscopic disks we use the results of Refs. 18 and 31 which allowed us to solve the problem semianalytically.

III. CHARGE IN THE MEISSNER AND THE GIANT VORTEX STATES

First, we consider the situation with a fixed value of the vorticity L. The giant vortex state has cylindrical symmetry and consequently the order parameter can be written as $\psi(\vec{\rho})=f(\rho)\exp(iL\theta)$. For a thin disk (case III) the order parameter is[31]

$$\psi(\rho,\theta)=\left(-\Lambda\frac{I_2}{I_1}\right)^{1/2} f_L(\rho)\exp(iL\theta), \tag{9}$$

where

$$f_L(\rho)=\left(\frac{H\rho^2}{2}\right)^{L/2}\exp\left(-\frac{H\rho^2}{4}\right)M\left(-\nu,L+1,\frac{H\rho^2}{2}\right), \tag{10}$$

$$I_1=\int_0^R \rho d\rho f_L^4(\rho), \quad I_2=\int_0^R \rho d\rho f_L^2(\rho), \tag{11}$$

$$\Lambda=H(1+2\nu)-1. \tag{12}$$

Here $M(a,b,y)$ is the Kummer function[32] and the value of ν is determined by the nonlinear equation, which results from the boundary condition (6):

$$\left(L-\frac{\Phi}{2}\right)M\left(-\nu,L+1,\frac{\Phi}{2}\right)-\frac{\nu\Phi}{L+1}M\left(-\nu+1,L+2,\frac{\Phi}{2}\right)=0. \tag{13}$$

Here $\Phi=HR^2$ is the magnetic flux through the disk in the absence of any flux expulsion. Using Eqs. (9)–(12) we can derive explicitly the charge distribution

$$\begin{aligned}q(\rho)=4\Lambda\frac{I_2}{I_1}\left(\frac{H}{2}\right)^L\rho^{2(L-1)}\exp\left(-\frac{H\rho^2}{2}\right)\Bigg\{&L^2M^2\left(-\nu,L+1,\frac{H\rho^2}{2}\right)-\frac{H\rho^2}{2}(2L+1)M\left(-\nu,L+1,\frac{H\rho^2}{2}\right)\Bigg[M\left(-\nu,L+1,\frac{H\rho^2}{2}\right)\\&+\frac{2\nu}{L+1}M\left(-\nu+1,L+2,\frac{H\rho^2}{2}\right)\Bigg]+\left(\frac{H\rho^2}{2}\right)^2\Bigg[M^2\left(-\nu,L+1,\frac{H\rho^2}{2}\right)+\frac{4\nu}{L+1}M\left(-\nu,L+1,\frac{H\rho^2}{2}\right)\\&\times M\left(-\nu+1,L+2,\frac{H\rho^2}{2}\right)+\frac{2\nu^2}{(L+1)^2}M^2\left(-\nu+1,L+2,\frac{H\rho^2}{2}\right)-\frac{2\nu(\nu+1)}{(L+1)(L+2)}\\&\times M\left(-\nu,L+1,\frac{H\rho^2}{2}\right)M\left(-\nu+2,L+3,\frac{H\rho^2}{2}\right)\Bigg]\Bigg\},\end{aligned} \tag{14}$$

where the charge density is measured in units of $q_0=\hbar^2/(16\pi m^* e\xi^4)=(a_B/32\pi\xi^4)e$ ($a_B=\hbar^2/me^2\approx 0.053$ nm is the Bohr radius). Notice that q_0 depends only on the material. For example, for Al [$\xi\simeq 250$ nm (Ref. 15)] we have $q_0/e\simeq 1.3\times 10^{-13}$ nm^{-3}, whereas for HTS materials ($\xi\simeq 1$ nm) it results in $q_0/e\simeq 5.3\times 10^{-4}$ nm^{-3}.

A. Meissner state

First, we study the Meissner state, i.e., $L=0$. The radial dependences of the Cooper pair density (or the corresponding distribution of the potential $\varphi(\rho)$ [see Eq. (1)]), the charge density $q(\rho)$, and the density of superconducting current $j(\rho)$ are shown in Figs. 1(a)–1(c) for the cases of cylinder, finite disk, and very thin disk, respectively, having the same radius $R=4.0\xi$ for different values of the applied field. Figure 1(d) shows these dependences for the same cylinder at the field $H=0.52H_{c2}$ but for different κ values. Due to the finite radial size of the samples, all distributions are inhomogeneous along the radius of the sample. The Cooper pair density is maximum at the center and decays towards the sample edge. As a result, in the center of the sample there is a region of positive charge while near the edge a negative ''screening'' charge q_{scr} is created. To avoid confusion let us note that for simplicity we write ''positive charge'' instead of ''charge of the same sign as is the sign of the dominant charge carriers.'' In the cylinder the Cooper pair density decreases with increasing field, while both the screening superconducting current and the charge polarization monotonously increase. The behavior for the disks is more complicated. For small fields the picture is very similar to the one of the cylinder. But for fields where the Meissner state becomes metastable [i.e., $H/H_{c2}>0.32$ for the parameters used in Fig. 1(b)] the screening charge becomes maximal. The positive charge is pulled further towards the center of the disk and the screening charge region expands. Notice that now the maximum of the positive charge decreases with field and also at the surface its absolute value decreases. For a cylinder, at fixed field but with increasing κ [Fig. 1(d)] its charge distribution behaves similar as for fixed κ and increasing magnetic field [see Fig. 1(a)].

Notice that even for $L=0$ when no vortex is present inside the superconductor, there is still a nonuniform charge distribution. This charge redistribution can be characterized by two quantities: (i) the distance ρ^* which separates the positive and negative charge regions and (ii) the total screening charge $Q_{-,scr}$ which is defined by the integral over the region V_- occupied by the negative charge:

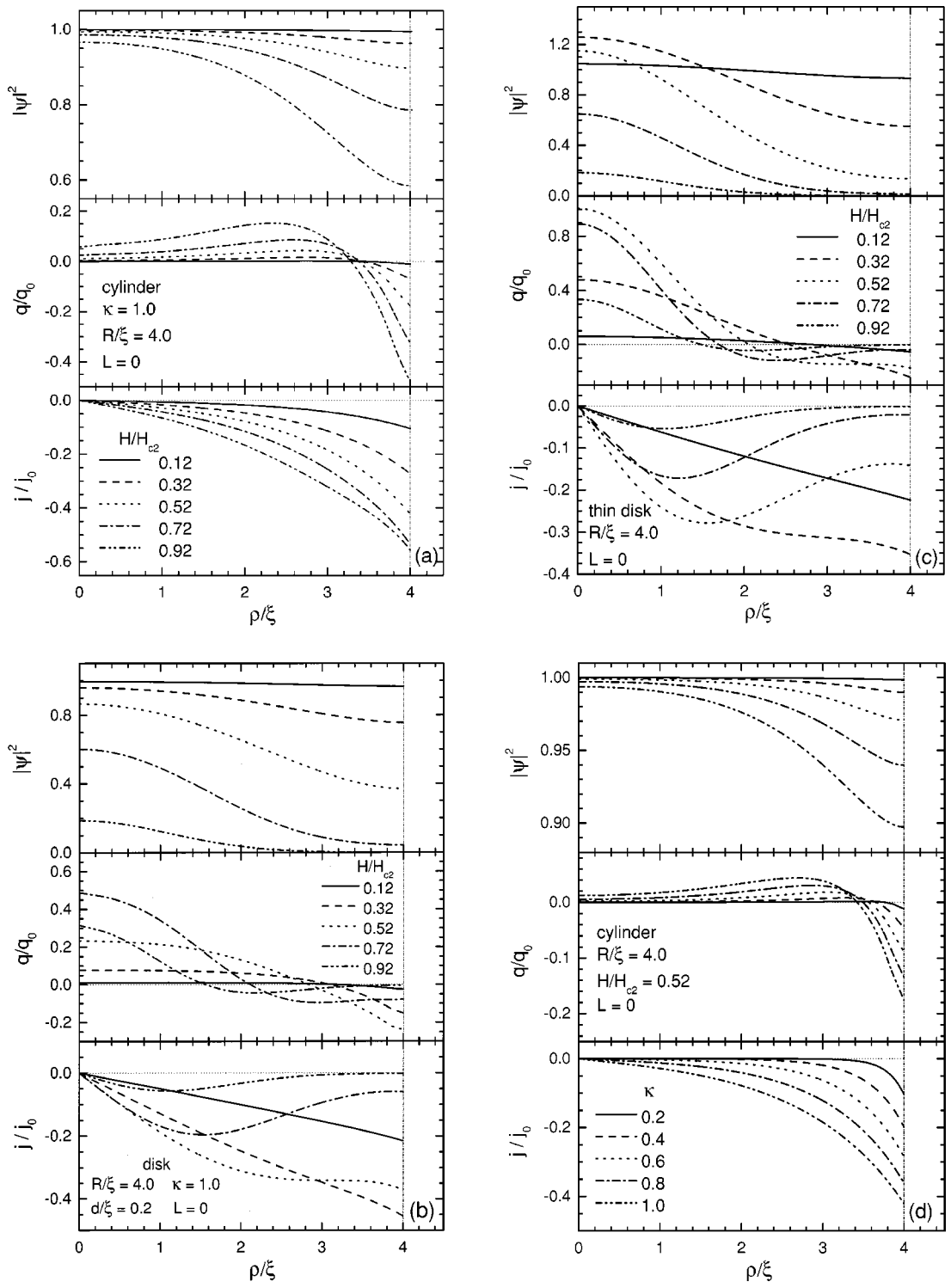

FIG. 1. The radial dependences of the Cooper pair density $|\psi(\rho)|^2$, the charge density $q(\rho)$, and the supercurrent density $j(\rho)$ in the Meissner state for (a) an infinitely long cylinder with $\kappa=1.0$, (b) a finite thickness disk with $d/\xi=0.2$, $\kappa=1.0$, (c) a very thin disk for different magnetic fields, and (d) an infinitely long cylinder with different Ginzburg-Landau parameter κ at the magnetic field $H=0.52H_{c2}$. All samples have the same radius $R/\xi=4.0$.

$$Q_{-,scr}=2\pi d\int_{(\rho_-)}\rho q_{scr}(\rho)d\rho. \tag{15}$$

The dependences of $\rho^*(H)$ are shown in Figs. 2(a)–2(c) for the cylinder, finite disk, and thin disk, respectively. In Fig. 2(c) the open squares refer to the magnetic field region where the $L=0$ state is metastable (the crossed circles will be explained below). Notice that ρ^* decreases with increasing field and this decrease is more pronounced for thinner disks. The magnetic field dependences of the absolute value

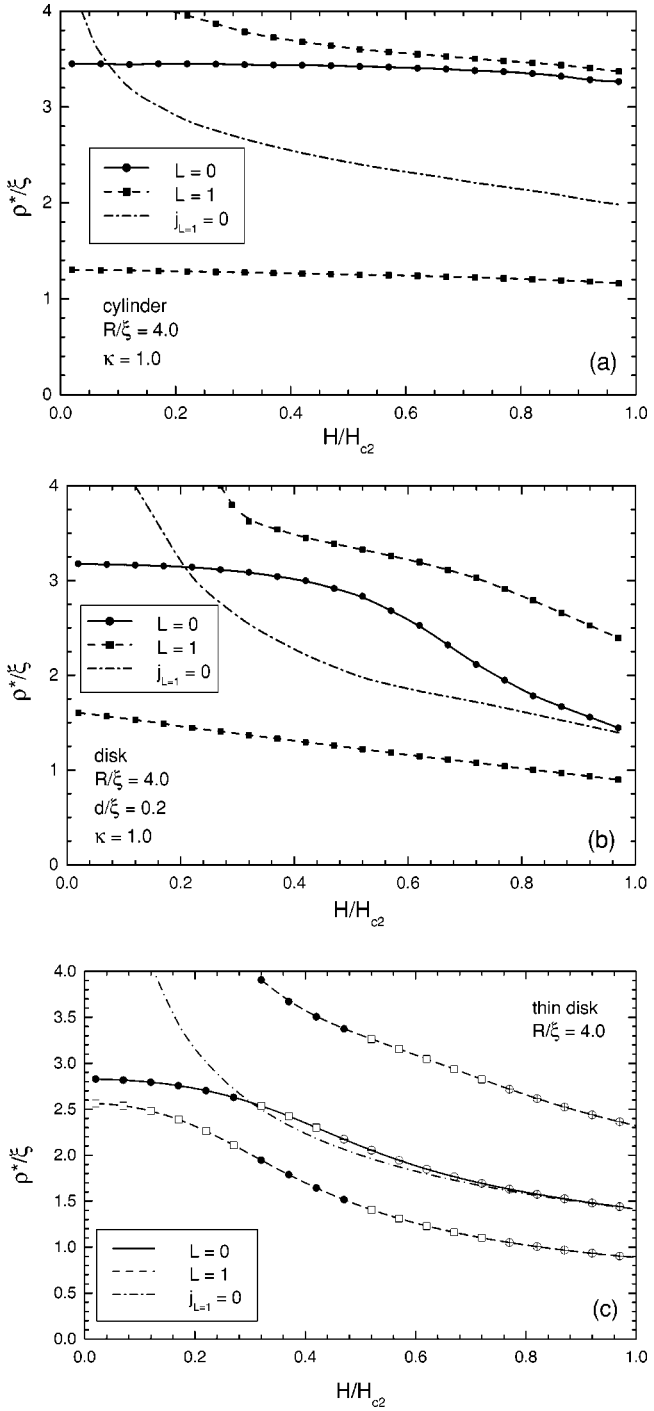

FIG. 2. The position of the boundary between the regions of negative and positive charges inside the sample as a function of the external magnetic field for (a) an infinitely long cylinder with $\kappa = 1.0$, (b) a finite-thickness disk with $d/\xi = 0.2$, $\kappa = 1.0$, and (c) a thin disk. The $\rho^*(H)$ dependences for the Meissner state are shown by the solid line and for the vortex state by the dashed lines. The dash-dotted curves represent the position of zero current.

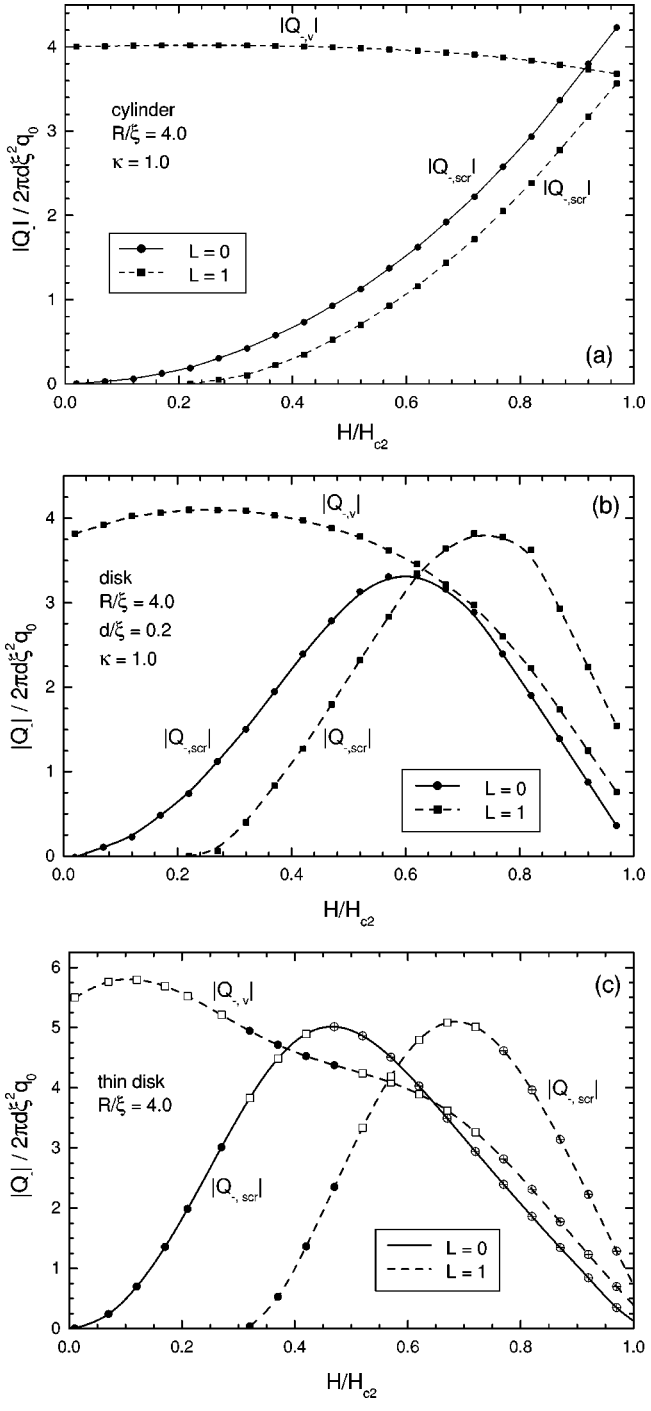

FIG. 3. The absolute value of the negative charge inside the sample as a function of the external magnetic field for (a) an infinitely long cylinder with $\kappa = 1.0$, (b) a finite-thickness disk with $d/\xi = 0.2$, $\kappa = 1.0$, and (c) a thin disk. The dependences for the Meissner state are shown by the solid line and for the vortex state by the dashed lines.

$|Q_-|$ of the screening charge is shown in Figs. 3(a)–3(c) for the same geometries. The screening charge Q_{scr} increases with magnetic field, but for the disk cases a local maximum is reached. This local maximum is reached for fields where ρ^* starts to decrease more strongly. From Figs. 3(a)–3(c) we notice that the linear screening charge density has approximately the same maximum values for all considered geometries. The total screening charge is determined by the coherence length ξ and the sample thickness d. For example, for a disk with $d = 0.2\xi$ (case II) we obtain for the screening charge $|Q_{-,scr}| \simeq 3 \times 2\pi\xi^2 q_0 d \simeq (d/\xi^2) \times 10^{-2}$ e nm at the

field $H=0.6H_{c2}$. For an Al disk ($\xi\simeq 250$ nm) it gives $|Q_{-,scr}|\simeq 8\times 10^{-6}\ e$. For strongly type-II superconductors which have a very small coherence length ξ as well as for sufficiently thick samples this induced charge can be made orders of magnitude larger: for a HTS disk ($\xi\simeq 1$ nm) with the same size $d=0.2\xi$ it increases up to $2\times 10^{-3}\ e$. This value and the corresponding linear screening charge density are of the same order of magnitude as the previous estimates for the vortex charge in bulk superconductors.[5,6,8,12]

By direct integration of $q(\rho)$ over the sample surface we find that the total charge per unit of sample length $Q=\oint d\theta\int_0^R \rho q(\rho)d\rho=0$; i.e., there is charge neutrality over the whole sample. But this fact can be easy generalized analytically for states with any vorticity. The proof is given in the Appendix.

B. Giant vortex state

The same dependences as in Figs. 1(a)–1(d) are shown in Figs. 4(a)–4(d) for samples in the $L=1$ vortex state. In this state $|\psi(\rho)|^2=0$ in the center of the vortex core located in the center of the sample. Notice that for a cylinder the charge distribution almost does not change with magnetic field. The reason is that the external field affects the Cooper pair density only near the sample edge region. This is different for the disk geometry, where large demagnetization effects strongly influence the penetration of the magnetic field in the disk which changes the vortex structure. The vortex core is negatively charged and at small fields the positive charge outside the vortex extends up to the border of the sample. The dependences of the position $\rho^*(H)$ and the size of the charge pileup $|Q_-|(H)$ for the $L=1$ state are shown in Figs. 2(a)–2(c) and 3(a)–3(c).

With increasing external magnetic field the screening current at the sample surface increases and makes the region near the border of the sample negatively charged. In this case there exist two ρ^*, where $q(\rho^*)=0$. The core of the vortex is negatively charged with total charge $|Q_{-,v}|$. Around this core there is a ring of positive charge which compensates the charge of the vortex core and the surface charge. Near the surface a ring of negative screening charge exists with total charge $|Q_{-,scr}|$. The size of the latter increases with increasing magnetic field. For disks, $|Q_{-,scr}|$ reaches a local maximum after which it decreases in the large magnetic field region; this is the region where the $L=1$ state is unstable [see the circles with crosses in Fig. 3(c)].

Next we investigated the charge distribution for the vortex states with $L>1$ and we limited ourselves to the thin disk case. From Eq. (14) one finds immediately that $q=0$ in the center of the disk when $L\geqslant 2$. Consequently, the charge distribution in the vortex core has a ring shape. To illustrate this we show in Figs. 5(a) and 5(b) the same dependences as in Fig. 4(c) but now for $L=2$ and 3, respectively. With the exception of the core region the charge distribution for the giant vortex states is qualitatively similar to the case $L=1$, and the charge on the sample surface changes sign with increasing external magnetic field. Notice also that the number of areas where the charge changes its sign does not increase with L: it equals 2 for small fields and increases to 3 for higher magnetic fields.

As a conclusion of this section, we found that the value of the screening charge also depends on the radial size of the sample but less strongly than on ξ and d. For example, increasing the radius of a thin disk (case III) from $R=4.0\xi$ to $R=8.0\xi$ we obtain a charge $|Q_{-,scr}|$ which is 3 (5) times larger for the states with $L=0$ ($L=1$).

IV. VORTEX CHARGE IN THE MULTIVORTEX STATE

For sufficiently large radial size of the superconductor the giant vortex state can break up into multivortices.[18–20] To explain the physics we limit ourselves to the case of a thin disk. It was shown[19,20] that the order parameter of the multivortex state in general can be viewed as a superposition of giant vortex states with different L_j:

$$\psi(\vec{\rho})=\sum_{L_j=0}^{L} C_{L_j} f_{L_j}(\rho)\exp(iL_j\theta), \tag{16}$$

where L is now the value of the effective total angular momentum which equals the number of vortices in the disk. For disks with not so large a radius $[(3-5)\xi]$ the order parameter of the multivortex state is the superposition of only two states and is described by the expression[31]

$$\psi(\vec{\rho})=C_{L_1} f_{L_1}(\rho)\exp(iL_1\theta)+C_{L_2} f_{L_2}(\rho)\exp(iL_2\theta), \tag{17}$$

where

$$C_{L_1}=\left(\frac{-\Lambda_{L_1}A_{L_2}B_{L_1}+2\Lambda_{L_2}A_{L_1,L_2}B_{L_2}}{A_{L_1}A_{L_2}-4A_{L_1,L_2}^2}\right)^{1/2}, \tag{18}$$

$$C_{L_2}=\left(\frac{-\Lambda_{L_2}A_{L_1}B_{L_2}+2\Lambda_{L_1}A_{L_1,L_2}B_{L_1}}{A_{L_1}A_{L_2}-4A_{L_1,L_2}^2}\right)^{1/2},$$

$$A_{L_i}=\frac{2\pi d}{V}\int_0^R \rho d\rho f_{L_i}^4(\rho),$$

$$A_{L_1,L_2}=\frac{2\pi d}{V}\int_0^R \rho d\rho f_{L_1}^2(\rho) f_{L_2}^2(\rho),$$

$$B_{L_i}=\frac{2\pi d}{V}\int_0^R \rho d\rho f_{L_i}^2(\rho), \tag{19}$$

and $f_{L_i}(\rho)$ and Λ_{L_i} are determined by Eqs. (10) and (12), respectively. The charge density distribution is then given by the expression

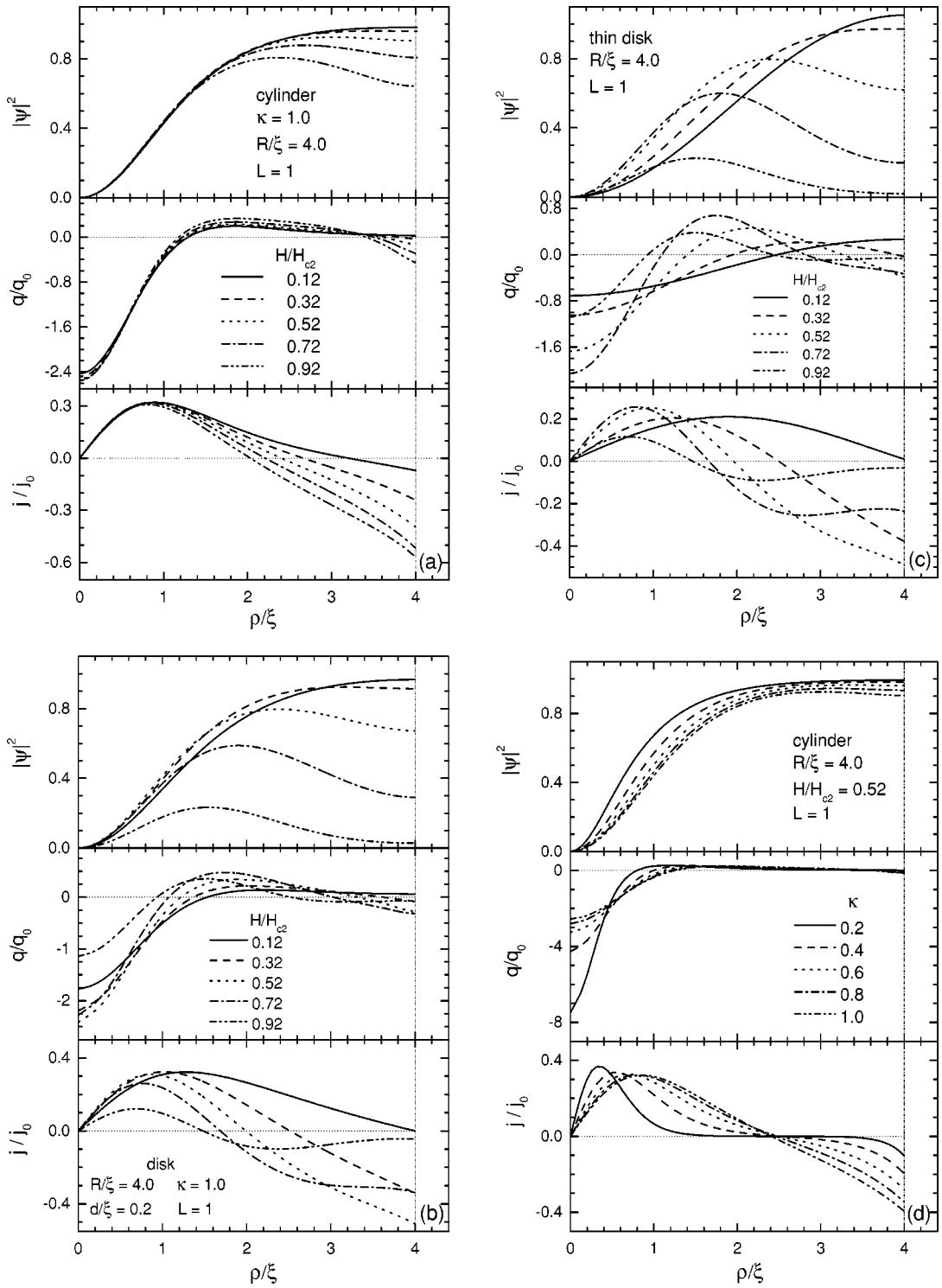

FIG. 4. The same as in Fig. 1 but for the single-vortex state (with $L=1$).

$$q(\rho,\theta)=2C_{L_1}^2\left[f_{L_1}'^2(\rho)+f_{L_1}(\rho)f_{L_1}''(\rho)+\frac{1}{\rho}f_{L_1}(\rho)f_{L_1}'(\rho)\right]$$
$$+2C_{L_2}^2\left[f_{L_2}'^2(\rho)+f_{L_2}(\rho)f_{L_2}''(\rho)+\frac{1}{\rho}f_{L_2}(\rho)f_{L_2}'(\rho)\right]$$
$$+2C_{L_1}C_{L_2}\cos[(L_1-L_2)\theta]\Bigg[f_{L_1}''(\rho)f_{L_2}(\rho)$$
$$+2f_{L_1}'(\rho)f_{L_2}'(\rho)+f_{L_1}(\rho)f_{L_2}''(\rho)+\frac{1}{\rho}[f_{L_1}'(\rho)f_{L_2}(\rho)$$
$$+f_{L_1}(\rho)f_{L_2}'(\rho)]-\frac{(L_1-L_2)^2}{\rho^2}f_{L_1}(\rho)f_{L_2}(\rho)\Bigg], \quad (20)$$

where the prime denotes the derivative with respect to ρ. The explicit expression is rather lengthy and is therefore not given here.

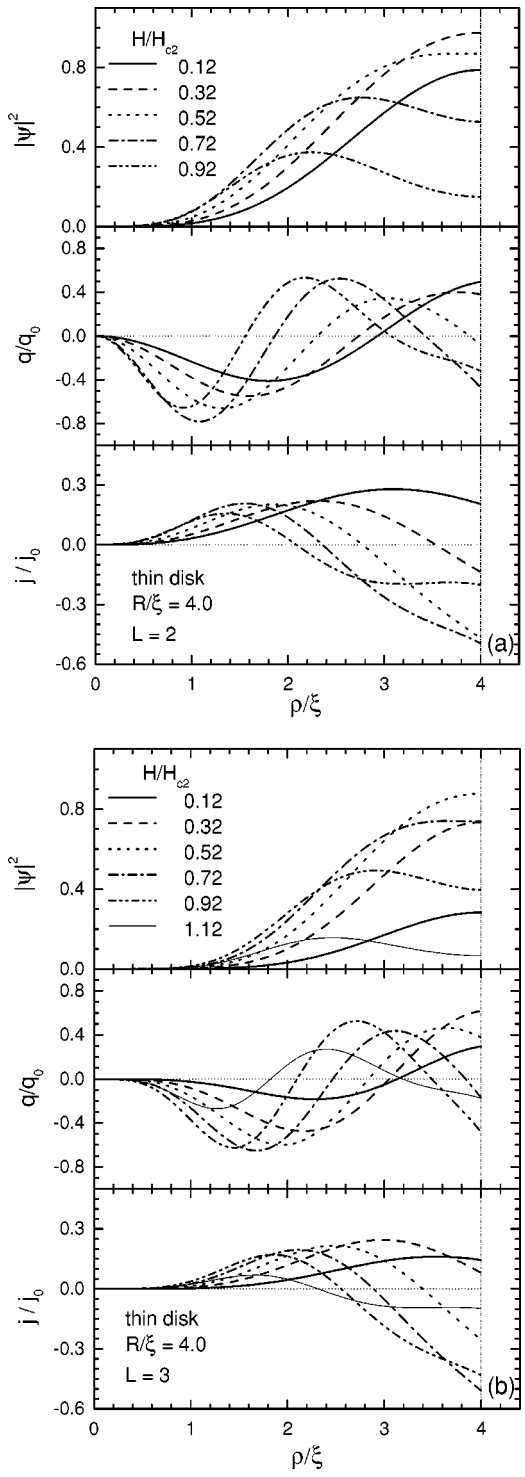

FIG. 5. The radial dependences of the Cooper pair density $|\psi(\rho)|^2$, the charge density $q(\rho)$, and the supercurrent density $j(\rho)$ in the giant vortex state with (a) $L=2$ and (b) $L=3$ for a thin disk with $R/\xi=4.0$ and for different applied magnetic fields.

Earlier analyses have shown[19,31,33] that there exist two kinds of multivortex states: (i) stable configurations which correspond to a minimum of the free energy and (ii) states which correspond to saddle points of the free energy. The latter ones correspond to the energy barrier states between states with different vorticity L and describe the penetration of flux into the disk. Due to the transitions between the different L states with increasing (or decreasing) external field, some giant vortex states are never realized [for example, such states for $L=0$ and 1 correspond to the crossed circles in Figs. 2(c) and 3(c)].

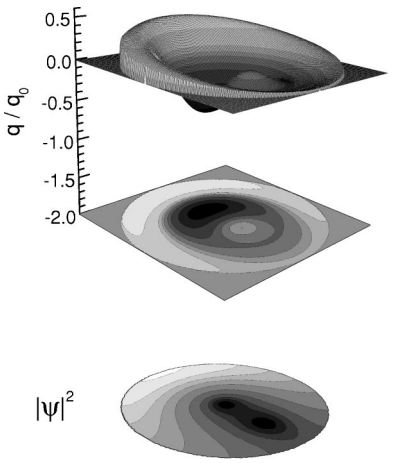

FIG. 6. The charge density distribution for the (1:2) saddle-point state at the field $H=0.32H_{c2}$ for a thin disk with $R/\xi=4.0$. The bottom contour plot shows the distribution of the Cooper pair density.

As an example, we consider a thin disk with $R/\xi=4.0$. The charge density $q(x,y)$ distributions over the disk for the different kinds of multivortex states are shown in Figs. 6 and 7. In Fig. 6 this distribution is given for the saddle point state (1:2) at the field $H=0.32H_{c2}$ and the contour plot of the distribution of the Cooper pair density $|\psi|^2$ for this state is shown at the bottom of the figure. The dark regions on the $|\psi|^2$ contour plot correspond to low Cooper pair density. The same distributions for the stable multivortex state (0:4) at the field $H=0.75H_{c2}$ are shown in Fig. 7. In general, the charge profiles are complicated enough, but nevertheless, one can see regions of negative charge located at the vortex core and positive charge near the edge of the sample. Using Eqs.

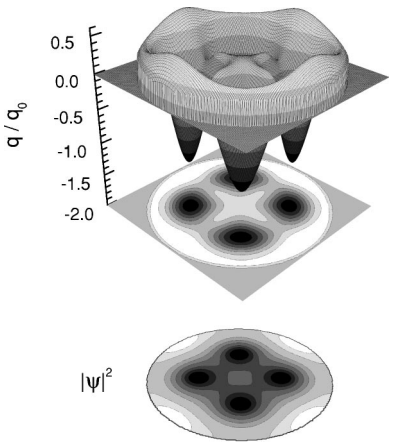

FIG. 7. The same as in Fig. 6 but for the (0:4) multivortex state in a disk with $R/\xi=4.0$ at the field $H=0.75H_{c2}$.

(17)–(19) it is easy to prove that also in the multivortex state the disk is electrically neutral as a whole (see also the Appendix).

V. CONCLUSIONS

We studied theoretically the redistribution of electrical charge in circular *mesoscopic* superconducting samples with different shapes, i.e., disks and cylinders. The theory applies for intermediate temperatures where the Ginzburg-Landau theory still gives reasonable results and where the share of superconducting electrons is already of order unity so that the screening by normal electrons may be neglected. Previously, it was predicted that the *vortex core* in bulk type-II samples is negatively charged. We found that in mesoscopic samples, in contrast to the bulk ones, even in the Meissner state *with no vortices* inside the sample, there exists a *nonuniform charge* distribution. Due to the finite radial size, a region near the sample edge becomes negatively charged while the interior of the sample has a corresponding positive charge. This charge redistribution is a consequence of the screening currents near the sample edge which makes it behave like a vortex which is turned inside out. When vortices are inside the sample there is a superposition of the vortex charge and this Meissner charge. Because of this interplay between vortex charge, which is positive near the sample surface, and the Meissner charge, which is negative at the sample surface, the charge at the sample edge *changes sign* as a function of the applied magnetic field. These effects become more pronounced with decreasing sample thickness. We also proved analytically that there is only a redistribution of charge and that the total sample charge is neutral as long as the boundary condition (6) is satisfied.

Finally, let us briefly discuss the possibility of experimental detection of the above screening charge. Recently, the vortex charge in a high-temperature YBaCuO superconductor was detected by the nuclear magnetic resonance (NMR) method.[12] The detection of vortex charge in type-II superconductors by the method of scanning tunneling microscopy (STM) has been discussed in detail by Blatter *et al.*[6] An alternative approach was proposed by Mishonov[34] using a transport measurement in a layered metal-insulator-superconductor system. As we have seen, the calculated values of the screening charge for mesoscopic samples are of the same order of magnitude as the vortex charge estimated for bulk type-II superconductors,[5,6,8] and, consequently, they are in the limits of accuracy of the above experimental techniques. On the other hand, some experience in the preparation and measurement of mesoscopic disks made from normal[15] and (Ref. 35) HTS materials also exists. Therefore, we believe that the NMR and STM methods can be used to probe the vortex electric charge in mesoscopic samples.

ACKNOWLEDGMENTS

This work was supported by the Flemish Science Foundation (FWO-Vl), the Belgian Inter-University Attraction Poles (IUAP-VI), the ''Onderzoeksraad van de Universiteit Antwerpen,'' and the ESF program on ''Vortex Matter.'' We are grateful to Yu. V. Medvedev for bringing Ref. 3 to our attention.

APPENDIX: PROOF OF ELECTRICAL NEUTRALITY IN A MESOSCOPIC SAMPLE

Using Eqs. (1) and (2) and the Gauss theorem the total charge Q can be expressed as

$$\begin{aligned} Q &= -\frac{|\alpha|}{8\pi e}\int_V \nabla^2 |\psi(\vec{r})|^2 dV \\ &= -\frac{|\alpha|}{8\pi e}\int_S \vec{\nabla}|\psi(\vec{r})|^2 d\vec{S} \\ &= -\frac{|\alpha|}{8\pi e}\int_S \vec{n}\cdot[\psi^*(\vec{r})\vec{\nabla}\psi(\vec{r}) + \psi(\vec{r})\vec{\nabla}\psi^*(\vec{r})]dS \\ &= -\frac{|\alpha|}{8\pi e}\int_S \vec{n}\cdot[\psi^*(\vec{r})(\vec{\nabla} - i\vec{A})\psi(\vec{r}) \\ &\quad + \psi(\vec{r})(\vec{\nabla} + i\vec{A})\psi^*(\vec{r})]dS. \end{aligned} \tag{A1}$$

From the boundary condition (6) and its complex conjugate it follows immediately that $Q \equiv 0$. Notice that this result is very general; it is valid for any vortex configuration (the giant vortex states and the multivortex ones) and arbitrary shape of the superconducting sample as long as the boundary condition (6) is satisfied.

For a superconductor in contact with a normal metal or for a surface enhancement of superconductivity[31] we have the more general boundary condition[28]

$$\vec{n}\cdot(-i\vec{\nabla} - \vec{A})\psi|_S = \frac{i}{b}\psi|_S. \tag{A2}$$

The phenomenological parameter b is a surface extrapolation length which is the effective penetration depth of the order parameter into the surrounding medium. The case $b<0$ corresponds to surface enhancement of superconductivity[31] and the opposite case $b>0$ corresponds to the superconductor-normal metal boundary. In these cases the sample should have the finite total charge

$$Q = \frac{|\alpha|}{4\pi e b}\int_S |\psi(\vec{r})|^2 dS = \frac{a_B}{16\pi\xi^2 b} e \int_S |\psi(\vec{r})|^2 dS. \tag{A3}$$

The value of this charge is determined by the both sample sizes and ξ as well as the charge sign is, determined by the sign of b.

*Permanent address: Donetsk Physical & Technical Institute, National Academy of Sciences of Ukraine, Donetsk 83114, Ukraine.

†Electronic address: francois.peeters@ua.ac.be

[1] F. London, *Superfluids* (Wiley, New York, 1950), Vol. I, Sec. 8.

[2] L. D. Landau and E. M. Lifshitz, *Fluid Mechanics* (Pergamon, Oxford, 1982), Sec. 1.

[3] Yu.M. Ivanchenko and A.N. Omel'yanchuk, Sov. J. Low Temp. Phys. **11**, 490 (1985).

[4] A.G. Van Vijfeijken and F.A. Staas, Phys. Lett. **12**, 175 (1964).

[5] D.I. Khomskii and A. Freimuth, Phys. Rev. Lett. **75**, 1384 (1995).

[6] G. Blatter, M. Feigel'man, V. Geshkenbein, A. Larkin, and A. van Otterlo, Phys. Rev. Lett. **77**, 566 (1996).

[7] M.A.R. LeBlanc, Supercond. Sci. Technol. **10**, 929 (1997).

[8] J. Koláček, P. Lipavský, and E.H. Brandt, Phys. Rev. Lett. **86**, 312 (2001).

[9] A.S. Alexandrov, Phys. Rev. B **60**, 14 573 (1999).

[10] J.E. Hirsch, cond-mat/0012517 (unpublished).

[11] J. Gorio, Phys. Rev. B **61**, 4222 (2000); M. Matsumoto and R. Heeb, cond-mat/0101155 (unpublished).

[12] K. Kumagai, K. Nozaki, and Y. Matsuda, Phys. Rev. B **63**, 144502 (2001).

[13] V.V. Moshchalkov, L. Gielen, C. Strunk, R. Jonckheere, X. Qiu, C. van Haesendonck, and Y. Bruynseraede, Nature (London) **373**, 319 (1995).

[14] V.A. Schweigert and F.M. Peeters, Phys. Rev. B **60**, 3084 (1999).

[15] A.K. Geim, I.V. Grigorieva, S.V. Dubonos, J.G.S. Lok, J.C. Maan, A.E. Filippov, and F.M. Peeters, Nature (London) **390**, 259 (1997).

[16] P.S. Deo, V.A. Schweigert, F.M. Peeters, and A.K. Geim, Phys. Rev. Lett. **79**, 4653 (1997).

[17] V.A. Schweigert and F.M. Peeters, Phys. Rev. B **57**, 13 817 (1998).

[18] V.A. Schweigert, F.M. Peeters, and P.S. Deo, Phys. Rev. Lett. **81**, 2783 (1998).

[19] V.A. Schweigert and F.M. Peeters, Phys. Rev. Lett. **83**, 2409 (1999).

[20] J.J. Palacios, Physica B **256-258**, 610 (1998); Phys. Rev. B **58**, R5948 (1998); Phys. Rev. Lett. **84**, 1796 (2000).

[21] E. Akkermans and K. Mallick, J. Phys. A **32**, 7133 (1999); E. Akkermans, D.M. Gangardt, and K. Mallick, Phys. Rev. B **62**, 12 427 (2000); **63**, 064523 (2001).

[22] P.S. Deo, F.M. Peeters, and V.A. Schweigert, Superlattices Microstruct. **25**, 1195 (1999).

[23] H.J. Fink and A.G. Presson, Phys. Rev. Lett. **151**, 219 (1966); Phys. Rev. **168**, 399 (1968).

[24] G.F. Zharkov, V.G. Zharkov, and A.Yu. Zvetkov, Phys. Rev. B **61**, 12 293 (2000); cond-mat/0008217 (unpublished); G.F. Zharkov, Phys. Rev. B **63**, 224513 (2001).

[25] H.J. Fink and V. Grünfeld, Phys. Rev. B **33**, 6088 (1986); A. Bezryadin, A. Buzdin, and B. Pannetier, *ibid.* **51**, 3718 (1995); E.M. Horane, J.I. Castro, G.C. Buscaglia, and A. López, *ibid.* **53**, 9296 (1996); V. Bruyndoncx, L. Van Look, M. Verschuere, and V.V. Moshchalkov, *ibid.* **60**, 10 468 (1999).

[26] B.J. Baelus, F.M. Peeters, and V.A. Schweigert, Phys. Rev. B **61**, 9734 (2000); F.M. Peeters, V.A. Schweigert, B.J. Baelus, and P.S. Deo, Physica C **332**, 255 (2000).

[27] V.M. Fomin, V.R. Misko, J.T. Devreese, and V.V. Moshchalkov, Phys. Rev. B **58**, 11 703 (1998).

[28] P. G. de Gennes, *Superconductivity of Metals and Alloys* (Addison-Wesley, New York, 1994).

[29] V.A. Schweigert and F.M. Peeters, Physica C **332**, 266 (2000).

[30] I. E. Tamm, *Fundamentals of the Theory of Electricity* (Mir, Moscow, 1979), p. 66.

[31] S.V. Yampolskii and F.M. Peeters, Phys. Rev. B **62**, 9663 (2000).

[32] *Handbook of Mathematical Functions*, edited by M. Abramovitz and I. Stegun (Dover, New York, 1970), p. 504.

[33] B.J. Baelus, F.M. Peeters, and V.A. Schweigert, Phys. Rev. B **63**, 144517 (2001).

[34] T. M. Mishonov, in *Superconducting and Related Oxides*; *Physics and Nanoengineering IV*, edited by D. Pavuna and I. Bozovic, [Proc. SPIE, **4048**, 97 (2000)].

[35] S.J. Bending, A.N. Grigorenko, R.G. Humphreys, M.J. Van Bael, J. Bekaert, L. Van Look, V.V. Moshchalkov, and Y. Bruynseraede, Physica C **341**, 981 (2000).